BRIEF DEFINITIVE REPORT

Clearance of cerebrospinal fluid from the sacral spine through lymphatic vessels

Qiaoli Ma[1], Yann Decker[2], Andreas Müller[3], Benjamin V. Ineichen[4], and Steven T. Proulx[1,5]

The pathways of circulation and clearance of cerebrospinal fluid (CSF) in the spine have yet to be elucidated. We have recently shown with dynamic in vivo imaging that routes of outflow of CSF in mice occur along cranial nerves to extracranial lymphatic vessels. Here, we use near-infrared and magnetic resonance imaging to demonstrate the flow of CSF tracers within the spinal column and reveal the major spinal pathways for outflow to lymphatic vessels in mice. We found that after intraventricular injection, a spread of CSF tracers occurs within both the central canal and the spinal subarachnoid space toward the caudal end of the spine. Outflow of CSF tracers from the spinal subarachnoid space occurred predominantly from intravertebral regions of the sacral spine to lymphatic vessels, leading to sacral and iliac LNs. Clearance of CSF from the spine to lymphatic vessels may have significance for many conditions, including multiple sclerosis and spinal cord injury.

Introduction

There has been a recent surge of interest in the anatomical pathways and physiology of cerebrospinal fluid (CSF) circulation and outflow. Traditional concepts such as an immune privilege of the central nervous system (CNS) and the absorption of CSF by arachnoid villi have been challenged by several findings that have highlighted an intimate role for the lymphatic system in these processes (Aspelund et al., 2015; Louveau et al., 2015; Engelhardt et al., 2017; Ma et al., 2017). A better understanding of the function of the lymphatic system in the clearance of CSF has relevance for many diseases, such as multiple sclerosis, neurodegenerative disorders, and hydrocephalus (Bakker et al., 2016; Da Mesquita et al., 2018; Louveau et al., 2018; Hsu et al., 2019).

In our previous studies, we have found using injections of inert macromolecular tracers into the lateral ventricle or cisterna magna of mice that a bulk flow of tracers proceeds through the basal cisterns to the lymphatic outflow pathways from the skull (Ma et al., 2017, 2019). Consistent with previous studies, CSF outflow was found to occur within sheaths of exiting cranial nerves to reach extracranial lymphatic vessels (McComb, 1983; Bradbury and Cserr, 1985; Koh et al., 2005). Despite previous reports to the contrary (Courtice and Simmonds, 1951), we found no evidence for CSF outflow directly to blood of inert tracers, even of low molecular weight (Ma et al., 2017). This led to the concept that outflow of CSF occurs through lymphatic vessels rather than to dural venous sinuses.

CSF has direct communication between the cranial and spinal compartments of the CNS through continuity of the subarachnoid space (SAS) at the foramen magnum. In addition, CSF freshly produced by the choroid plexuses has access to the spine through the central canal (CC) through an aperture on the floor of the fourth ventricle. The direction of flow of CSF in either the spinal SAS (Ishibashi, 1959; Di Chiro, 1966; Davson and Segal, 1996) or the CC (Bradbury and Lathem, 1965; Milhorat et al., 1991; Cifuentes et al., 1992; Liu et al., 2018) is controversial. Most of these studies were performed under anesthetized, immobilized conditions, which limits CSF circulation (Ma et al., 2019), or involved direct injections of tracers into the intrathecal space, which may artificially induce nonphysiological tracer distribution.

Several different CSF outflow pathways from the spine have been proposed. These include flow through arachnoid villi to spinal veins (Elman, 1923; Welch and Pollay, 1963; Kido et al., 1976), routes along spinal nerve roots to epidural lymphatics (Iwanow, 1928; Brierley and Field, 1948), and routes through the arachnoid layer of the spinal meninges to dural lymphatics (Zenker et al., 1994; Antila et al., 2017). Previous groups have estimated that 16–25% of total CSF outflow may occur from the spine (Marmarou et al., 1975; Bozanovic-Sosic et al., 2001; Asgari et al., 2017). Others have suggested that spinal outflow pathways to lymphatic vessels are not active under normal conditions and

....
[1]Institute of Pharmaceutical Sciences, Swiss Federal Institute of Technology, ETH Zurich, Zurich, Switzerland;   [2]Department of Neurology, University of the Saarland, Homburg, Germany;   [3]Clinic for Diagnostic and Interventional Radiology, University of the Saarland, Homburg, Germany;   [4]Brain Research Institute, University of Zurich, Zurich, Switzerland;   [5]Theodor Kocher Institute, University of Bern, Bern, Switzerland.

Correspondence to Steven T. Proulx: steven.proulx@tki.unibe.ch.

that pathways through the cranial outflow routes must be blocked and/or that CSF pressures need to be elevated to produce outflow (Miura et al., 1998; Voelz et al., 2007).

Thus, it is clear at this point that several fundamental questions remain unanswered regarding the circulation and outflow of CSF in the spine. Therefore, in this study we used noninvasive near-infrared and magnetic resonance imaging (MRI) methods after infusions of macromolecular tracers at minimal rates and volumes into the lateral ventricle of mice to examine the circulation of CSF in the spinal column and identify the major spinal outflow pathways. We demonstrate the existence of CSF movement toward the caudal end of the spine through both the CC and spinal SAS to lymphatic vessels draining the sacral region of the spine.

Results and discussion

Flow of tracers infused into the lateral ventricle occurs down the CC to the sacral spine

We first aimed to evaluate the distribution of 40-kD pegylated near-infrared IRDye680 (P40D680) tracer (Proulx et al., 2017) in the spine 60 min after intracerebroventricular (i.c.v.) infusion. Two areas of the spine that we defined as thoracic and sacral regions had apparent high tracer signals (Fig. 1, A and B). Due to the curvature of the spine, which made these particular regions more accessible to near-infrared imaging, it was not immediately clear if the tracer had spread to the sacral region through the spinal SAS or directly through the CC from the ventricles. To evaluate this question, we employed a noninvasive dynamic imaging approach. Starting at 5 min after infusion, one group of mice was imaged at the thoracic region, while another group was imaged at the sacral region (Fig. 1 C and Videos 1 and 2). Surprisingly, the sacral region, despite its distance from the lateral ventricle infusion site, exhibited an enhancement of signal starting at an average of 17.0 ± 2.3 min after infusion that was significantly faster than the initial enhancement of 23.7 ± 5.5 min at the thoracic region (Fig. 1 D), implying tracer transport down the CC.

As the entrance of the CC exists at the floor of the fourth ventricle, infusions of tracer into the lateral ventricle but not the cisterna magna should lead to tracer transport to the caudal spine (Bradbury and Lathem, 1965). To test this, we compared the P40D680 tracer signals at the sacral region of spine between mice in which tracer was infused i.c.v. or into the cisterna magna (i.c.m.; Fig. S1). Signals at the sacral region were significantly higher in the i.c.v. group compared with the i.c.m. group (i.c.v. 1,855 ± 874 vs. i.c.m. 374 ± 187 counts, P < 0.0001). No significant differences were apparent in the thoracic region, indicating that tracers have access to the SAS of the upper spine through either injection route (i.c.v. 7,231 ± 2,543 vs. i.c.m. 5,555 ± 3,600 counts, P = 0.388). We next aimed to provide histological evidence of tracer within the CC of the spinal cord after i.c.v. injection. Since P40D680 is not amenable to fixation, we used Evans blue (EB) dye, which can also be assessed using its fluorescence on spinal cord sections. 30 min after infusion, EB was clearly apparent in the CC of the thoracic spinal cord (Fig. 1 E). EB was also obvious in the SAS at this level of the spine. At the lumbar region, EB could still be detected in the CC, albeit with much weaker fluorescence (Fig. 1 F). This is likely due to its low molecular weight, as EB easily diffuses into the spinal parenchyma through the ependymal lining of the CC, similar to our previous observations at the brain ventricles (Ma et al., 2017). Together, these data indicate that a directional flow of CSF occurs within the CC from the ventricular system to the caudal end of the spine.

Tracer accumulates at intervertebral regions in the sacral region of the spine

We have previously shown that mice that were allowed to recover from anesthesia after infusion of tracers exhibited dramatically accelerated CSF dynamics (Ma et al., 2019). Therefore, we speculated that a similar experimental approach may lead to insights into CSF circulation in the spine. We infused P40D680 i.c.v. and allowed the mice to either recover from isoflurane anesthesia (awake group) or maintained them on a heating pad under anesthesia (isoflurane group). Experiments were also performed in a third group of mice anesthetized with ketamine/medetomidine (ket/med group). By varying the amount of time after the i.c.v. infusion (15, 30, 60, and 90 min), we examined how the dynamics of tracer distribution were altered between the awake and anesthetized conditions.

We first assessed the signals of the tracer within the thoracic region of the spine (Fig. 2, A and B). In mice allowed to awaken, the tracer spread to this region in greater quantity at early time points compared with ket/med-anesthetized mice. At later time points, the tracer signals decreased in the awake mice, indicating that the tracer was being cleared from the thoracic SAS. In ket/med-anesthetized mice, the tracer signals were first apparent at 30 min and then increased over time, indicating slower CSF dynamics under these conditions. Isoflurane-anesthetized mice demonstrated an intermediate pattern of tracer dynamics, with signals increasing up to 60 min before declining at 90 min.

Using this approach to examine the sacral region of the spine (Fig. 2 C), several interesting observations were made. First, the initial pattern of tracer signal exhibited focal accumulations in the regions between vertebrae. At later time points, the number of intervertebral regions containing tracer increased, with more enhanced regions found in the awake mice compared with anesthetized groups (Fig. 2 D). On examination of the mean fluorescent signals at the sacral region over time (Fig. 2 E), no significant differences were found at early time points between the three groups. Signals continued to increase in this region over time in all three groups of mice; however, signals in isoflurane-anesthetized mice were significantly higher than both the awake and ket/med-anesthetized groups at 90 min, indicating increased accumulation of tracer in this region under these conditions. Finally, obvious tracer-filled vessel-like structures that were most apparent in awake mice were seen emerging from the intervertebral regions, which led us to examine the potential CSF outflow pathways from the spine in detail.

Tracers clear through lymphatic vessels at the caudal end of the spine to reach sacral and iliac LNs

To demonstrate lymphatic outflow pathways from the spine, we imaged Prox1-GFP mice that were awake for 60 or 90 min after P40D680 i.c.v. infusion. On the dorsal aspect of the spine,
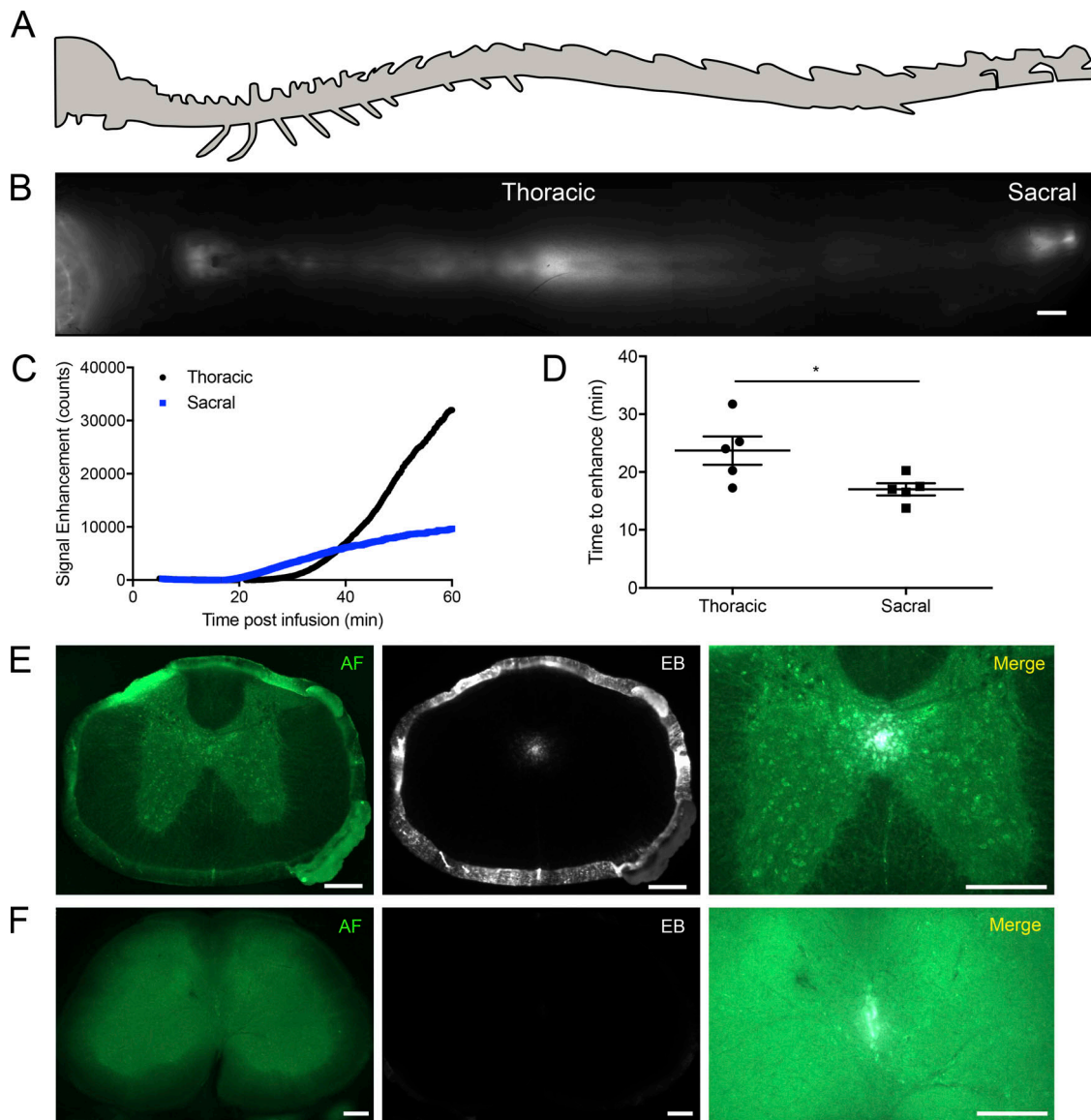
Ma et al.
Lymphatic clearance of CSF from the spine

Journal of Experimental Medicine
https://doi.org/10.1084/jem.20190351

2493

Figure 1. **A rapid flow of tracers occurs down the CC to the sacral spine. (A)** Schematic of spine (lateral view). **(B)** Composite image of the dorsal aspect of the spine demonstrating enhanced tracer signal in the thoracic and sacral regions 1 h after i.c.v. infusion of P40D680. Scale bar, 2 mm. **(C)** Representative signal dynamics of P40D680 tracer spread to the thoracic (black) and sacral (blue) regions after i.c.v. infusion. **(D)** Initial time of P40D680 signal enhancement to the thoracic and sacral regions from the i.c.v. infusion site. Data are mean ± SD and representative of two independent experiments (n = 5 each group, two-tailed Student's t test; *, P < 0.05). **(E)** Infusions of 0.6% EB i.c.v. were performed, and mice were sacrificed at 30 min. Representative section from the thoracic spinal cord showing the anatomic features from the green autofluorescence (AF) channel and demonstrating EB fluorescence signal in the CC, as well as on the pia mater lining the SAS. Scale bars, 200 μm. **(F)** Representative section from the lumbar spinal cord demonstrating EB in the CC, with no obvious EB fluorescence apparent in the SAS. Scale bars, 200 μm. Representative of three independent experiments.

tracer-filled Prox1-GFP⁺ lymphatic vessels emerged from the intervertebral regions (Fig. 3 A) and drained into afferent-collecting lymphatic vessels of sacral LNs. On the ventral side, we identified collecting lymphatic vessels along the axis of the spine from the sacral efflux sites draining tracer in a rostral direction toward the caudal mesenteric and/or iliac LNs (Fig. 3 B). Tracer within the efferent-collecting lymphatic vessels of the sacral LNs also drained to the iliac LNs, indicating that this LN group may be especially important for drainage of CSF from the spine. In other regions of the spine, minor presence of tracer in Prox1-GFP⁺ lymphatic vessels was occasionally detectable at the dorsal lumbar region (Fig. S2). More frequently, tracer-filled vessels emerged

from the dorsal sacral spine and tracked further caudally to the tail (Fig. S2). These lymphatic vessels then reversed course and drained to the inguinal LNs. A close examination of several other regions along the spine did not reveal any further sites of lymphatic outflow. Schemes of the anatomical routes of lymphatic outflow from the sacral spine are shown in Fig. 3, C and D.

Tracer outflow to spine-draining LNs is minor in comparison to outflow to cranial-draining LNs

We compared the average tracer signals within cranial-draining (mandibular and deep cervical) and spine-draining (iliac and caudal mesenteric) LNs at 60 min in the ket/med-anesthetized
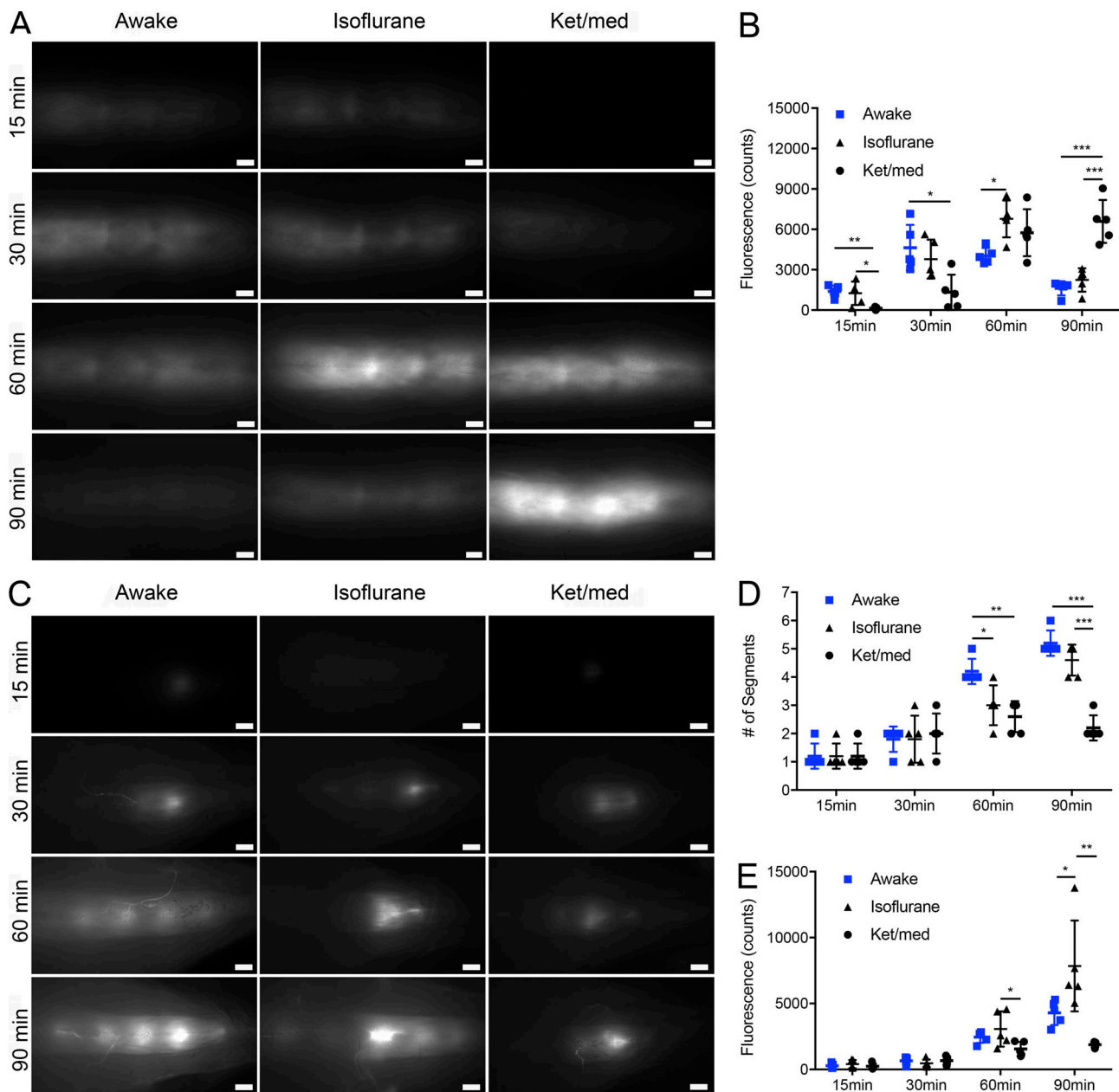
Figure 2. **Distribution of tracers within the thoracic and sacral spine under awake and anesthetized conditions. (A)** Representative pictures of tracer within the thoracic region of the spine after sacrifice at 15, 30, 60, and 90 min after P40D680 infusion into the right lateral ventricle of anesthetized (isoflurane and ket/med) and awake group mice. Scale bars, 1 mm. **(B)** Quantification of fluorescence intensity in the thoracic region at the different time points. **(C)** Representative pictures of tracer within the sacral region of the spine. Scale bars, 1 mm. **(D)** Quantification of the number of tracer-enhanced segments between vertebrae at the different time points in anesthetized and awake mice. **(E)** Quantification of fluorescence intensity in the sacral region at the different time points in anesthetized and awake mice. Data are mean ± SD and representative of two independent experiments (n = 5 each group, one-way ANOVA with Tukey post hoc test; *, P < 0.05; **, P < 0.01; ***, P < 0.001).

and awake groups (Fig. 4 A). In ket/med-anesthetized mice, the tracer signals within the spine-draining LNs were barely above background levels and far below the levels seen in the cranial-draining LNs (Fig. 4 B). Although lymphatic outflow was increased in awake mice with higher signals within the spine-draining LNs compared with ket/med-anesthetized mice (awake 2,837 ± 1,105 vs. ket/med 732 ± 601 counts, P < 0.0057), the tracer signals were still slight in comparison to the levels found in the cranial-draining LNs. We conclude that the

proportion of CSF draining through this route is far below the level that drains along the cranial nerves to the mandibular and deep cervical LN basins.

MRI validation of spinal CSF distribution and sacral lymphatic outflow after i.c.v. infusion

Finally, we aimed to confirm our findings with MRI. We developed a method to visualize both the ventricular system and the entire spinal column in mice within one three-dimensional
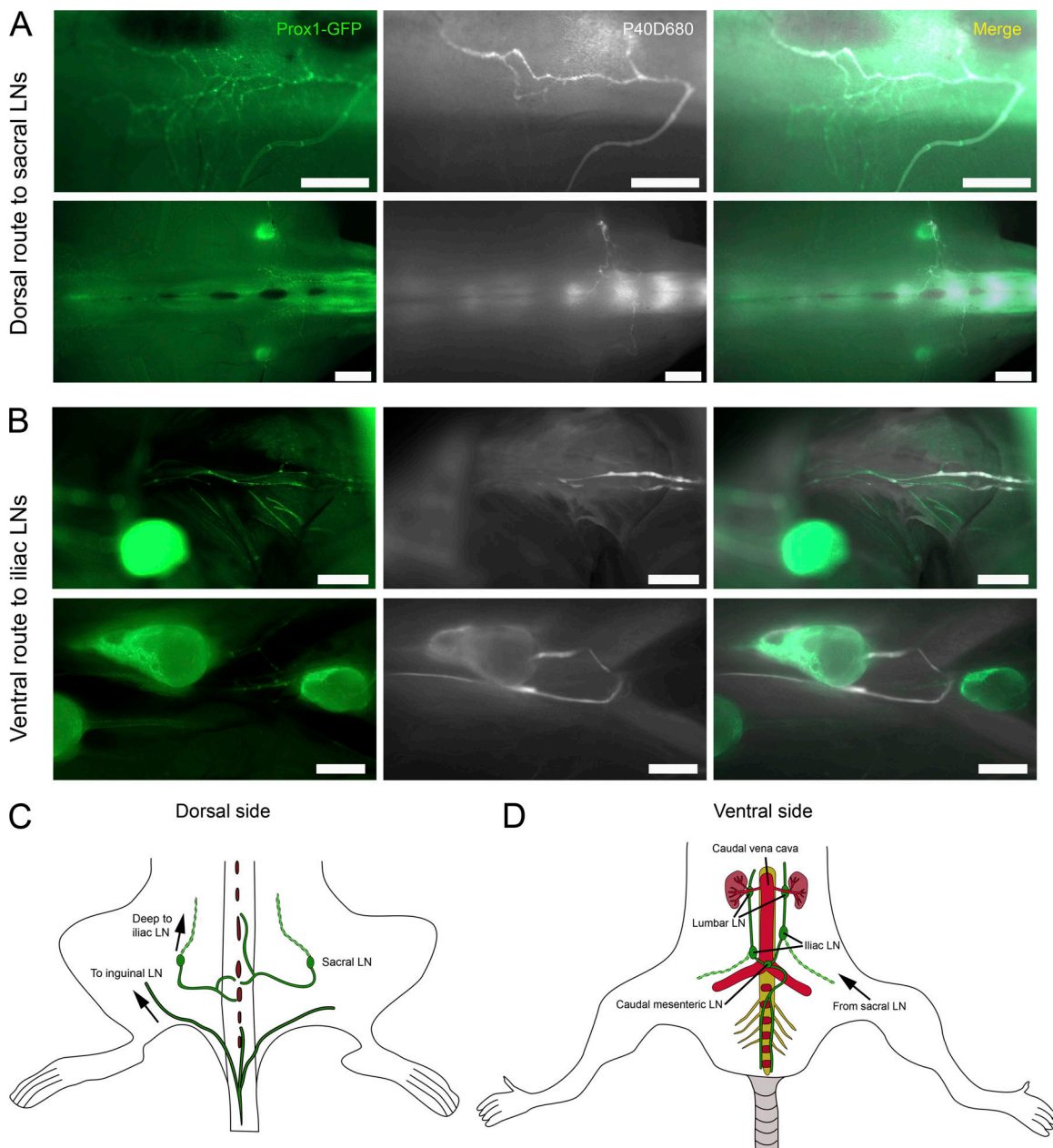
Figure 3. Tracers clear through lymphatic vessels at the caudal end of the spine. (A) Representative pictures of P40D680 tracer within Prox1-GFP⁺ lymphatic vessels in the dorsal aspect of the sacral spine. Images were acquired 60 min after P40D680 i.c.v. infusion in awake group mice. Scale bars, 1 mm (upper row); 2 mm (lower row). **(B)** Representative pictures of P40D680 tracer within Prox1-GFP⁺ lymphatic vessels running parallel along the ventral aspect of the lumbar spine. Scale bars, 1 mm. Data are representative of three independent experiments. **(C)** Schematic of lymphatic vessel routing from dorsal aspect of the caudal spine to sacral LNs. A route along subcutaneous lymphatic vessels from the base of the tail to inguinal LNs is also typically observed. **(D)** Schematic of lymphatic vessel routing on ventral aspect of the caudal spine to caudal mesenteric and iliac LNs.

(3D) scan and to perform infusions of contrast agents into the lateral ventricle through an implanted cannula while animals were positioned in the magnet. This allowed us to collect a baseline scan and then initiate a low-rate infusion (0.1 µl/min over the course of 60 min) of Gadospin D while performing scans every 6 min under isoflurane anesthesia.

Using this protocol, we found evidence of contrast agent flow down the CC, with simultaneous spreading of the contrast agent to the spinal SAS (Figs. 5 A and S3). This method also allowed 3D dynamic visualization of a lateral and dorsal spread of contrast

agent over time in the sacral intervertebral regions (Fig. 5, B and C). We were able to confirm lymphatic outflow to both sacral and iliac LNs (Fig. 5, A and C; Fig. S3; and Video 3). No lymphatic outflow pathways from other regions of the spine were apparent, although a slow diffusion of contrast agent along cervical nerve roots was visualized (Fig. 5 A). Finally, a delayed enhancement of Gadospin D in the bladder (Fig. S3) is consistent with lymphatic outflow of CSF (Ma et al., 2017). In sum, the MRI data has supported the concept of a caudal circulation of CSF in the spine to sites of lymphatic outflow in the sacral region.
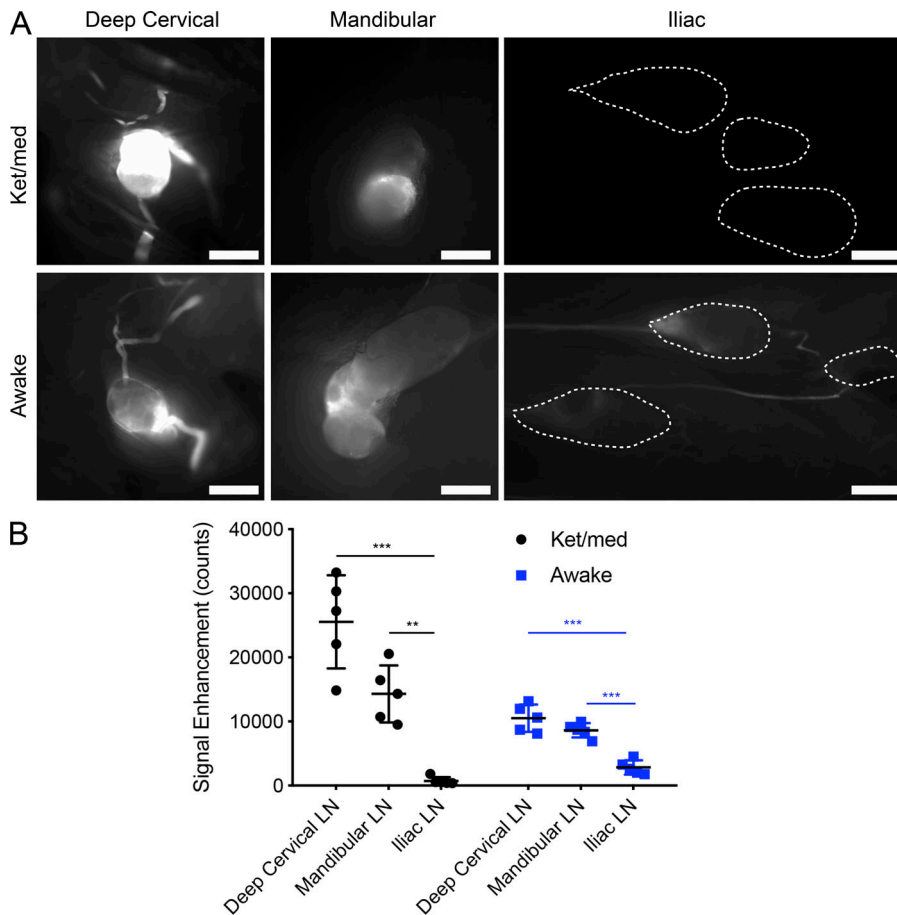
Figure 4. **Tracer outflow to spine-draining LNs is minor in comparison to outflow to cranial-draining LNs.** **(A)** Representative pictures of tracer within deep cervical, mandibular, and iliac/caudal mesenteric LN groups 60 min after P40D680 i.c.v. infusion in ket/med and awake mice. Dashed lines were drawn using Prox1-GFP signals to indicate the location of LNs with low P40D680 signal. Scale bars, 1 mm. **(B)** Fluorescence intensity of the three LN groups at 60 min in ket/med and awake mice. Data are mean ± SD and representative of two independent experiments (n = 5 each group, one-way ANOVA with Tukey's post hoc analysis; **, P < 0.01; ***, P < 0.001).

In this study, we have elucidated several aspects of CSF circulation in the spine using bulk flow tracers and imaging in mice. We found that a directional flow of CSF occurs through the CC from the ventricles to the caudal end of the spine and that under both awake and anesthetized conditions, a cranial-to-caudal movement of tracer also exists within the spinal SAS. This leads to tracer accumulation at intervertebral regions in the sacral spine, where outflow of CSF occurs through lymphatic vessels.

This study has provided strong evidence for a normal flow of CSF to the caudal aspect of the spine within the CC in mice. The direction of the flow of CSF within the CC is a controversial topic, as conflicting data have been published in the past (Bradbury and Lathem, 1965; Milhorat et al., 1991; Cifuentes et al., 1992; Liu et al., 2018). Our conclusion of a caudally directed flow is in close agreement with Bradbury and Lathem (1965) using rabbits and subsequent work in guinea pigs and rats (Nakayama, 1976; Cifuentes et al., 1992). We found that the tracer within the CC was able to access the sacral SAS as early as 15 min after infusion. Dorsal outlets for the fluid in the CC with connections from the filum terminale internum to the SAS have been identified in the sacral spine in rats, rabbits, guinea pigs, and rhesus monkeys (Leduc et al., 1956; Bradbury and Lathem, 1965; Nakayama, 1976). In humans, a normal flow within this anatomic space is often paid little heed, as it is believed that CC is occluded after the third decade of life (Saker et al., 2016). This is despite the well-known association between dilated CCs and the development of syringomyelia (Gardner and Goodall, 1950; Williams and Bentley, 1980).

The accepted driving forces for pulsatile CSF motion, respiration and arterial pulse (O'Connell, 1943; Du Boulay et al., 1972; Dreha-Kulaczewski et al., 2015), are not thought to exert a directional flow in the spine but instead to produce to-and-fro movements of fluid. In our study, tracer cleared from the SAS of the thoracic region in the awake and isoflurane-anesthetized mice at later time points, with a strong increase in signals at the sacral region at these same time points. Evidence for a caudal-directed movement of CSF has been previously shown in cats and monkeys (Grundy, 1962; Post et al., 1974). At this point, we cannot completely rule out that the tracer reaches the spinal SAS due to an acute rise in intracranial pressure during the bolus infusion. However, even under conditions of a low-rate (0.1 µl/min) infusion as performed during the MRI study, we were able to demonstrate a caudal movement of contrast agent in the spinal SAS.

Another major reason for the lack of acceptance for a directional flux of CSF in the spinal column is that there has been no confirmed anatomical route for outflow from this compartment of the CNS. Similar to the case with cranial arachnoid villi, in vivo physiological evidence for CSF efflux to spinal veins is lacking. Our results demonstrating a lymphatic outflow are in agreement with several previous studies that have shown evidence of tracers within spine-draining lymphatic vessels or LNs (Iwanow, 1928; Galkin, 1930; Brierley and Field, 1948; Woollam
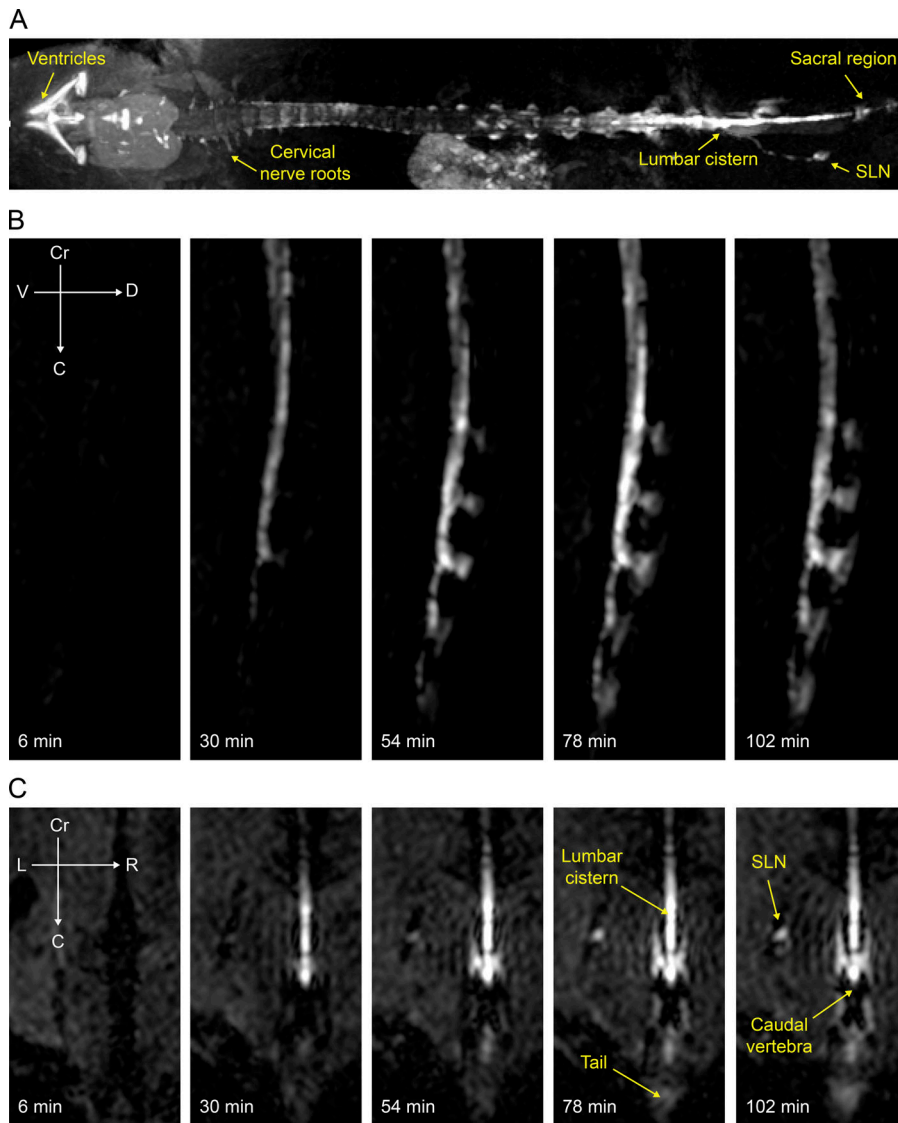
and Millen, 1958; Kida et al., 1993; Zenker et al., 1994; Boulton et al., 1996; Miura et al., 1998; Voelz et al., 2007; Kwon et al., 2017). These earlier investigators typically needed to employ multiple injections of tracer, to inject high volumes directly into the spinal SAS, or to block cranial outflow pathways to demonstrate spinal outflow to lymphatics. Here, we show with low-volume injections of tracer or contrast agent into the lateral ventricle that a spinal CSF outflow through lymphatics can be detected under more physiological conditions. This is in agreement with the classic work in rabbits from Brierley and Field (1948) using India ink and work from the group of Miles Johnston (Boulton et al., 1996) in sheep using radiolabeled albumin.

The detailed anatomy at the sites of outflow to lymphatics still needs elucidation. We speculate that the tracer-enriched regions between vertebral segments may represent outflow pathways at the subarachnoid angle (McCabe and Low, 1969). At these locations where the spinal nerve roots exit the spinal column, the arachnoid membrane forms a cul-de-sac at the root ganglion. In early studies, India ink particles were found to accumulate at the cul-de-sac, with some particles found within

nearby epidural lymphatics (Iwanow, 1928; Brierley and Field, 1948). It has been proposed that at this particular site the arachnoid barrier is lacking, providing potential access to lymphatic vessels located within the spinal dura mater or in epidural tissue (Zenker et al., 1994). While these networks of lymphatic vessels have been found to be particularly enriched at the cervical and thoracic regions (Antila et al., 2017; Jacob et al., 2019 *Preprint*; Miura et al., 1998), we could detect CSF outflow predominantly at the caudal end. Both postmortem near-infrared fluorescence imaging in Prox1-GFP mice and in vivo MRI indicated a lack of significant outflow at other spinal locations. We speculate that outflow pathways at the end of the spine would provide a potential sink of lower pressure that would help to distribute CSF from its site of production within the ventricles down the length of the spinal column. In humans, an outflow at the caudal end would perhaps be even more logical because our species spends a significant amount of time in an upright position.

Finally, we demonstrate that the proportion of CSF draining from the spine appears to be limited compared with outflow from the skull. It has been found that CSF outflow resistance

from the spine was far greater than that from the cranium, indicating that the spinal outflow pathways are less open to bulk flow (Bozanovic-Sosic et al., 2001). Supporting this concept, we found that tracer signals were still increasing in the sacral spine at 90 min in awake mice despite our earlier data indicating that up to 80% of the infused tracer has already reached the systemic blood under these conditions (Ma et al., 2019). Surprisingly, accumulation of tracers at 90 min in the sacral region was even greater in isoflurane-anesthetized mice. It is likely that this accumulation at the sites of spinal outflow under isoflurane represents a reduced clearance by lymphatics. Decreased lymphatic clearance may be due to the known effects of tissue immobilization during anesthesia on initial lymphatic uptake (Proulx et al., 2017) and inhibitory effects of isoflurane on the contractility of collecting lymphatic vessels (Bachmann et al., 2019). Despite the slow relative turnover of CSF in the spine, it is still evident that a normal CSF circulation occurs within this compartment of the CNS toward lymphatic outflow pathways.

The presence of caudally directed movement of CSF in the spinal column to sacral lymphatic outflow routes still needs to be confirmed in humans. This fluid pathway may have implications for diseases such as multiple sclerosis and syringomyelia, as well as after spinal cord injury. In addition, elucidation of the routes of circulation of CSF may lead to optimized strategies for CNS drug delivery and an improved interpretation of clinical sampling of CSF constituents from lumbar puncture.

Materials and methods

Mice
Female wild-type mice (Janvier) and Prox1-GFP reporter mice on the C57BL/6J background were kept under specific pathogen–free conditions and used for experimental studies at the age of 2–3 mo. Prox1-GFP mice were backcrossed to a C57BL/6J background for ≥10 generations. All mouse experiments were approved by the Kantonales Veterinäramt Zürich (license numbers 185/13, 161/16, and 245/17) and by the Landesamt für Gesundheit und Verbraucherschutz, Saarbruecken, Germany (license number 31/2018), and performed following the regulations of the Swiss Federal Welfare Act.

Infusion of tracers into lateral ventricle or cisterna magna
Mice were anesthetized (80 mg/kg ketamine and 0.2 mg/kg medetomidine or with 2% isoflurane) and positioned in a stereotaxic frame (RWD) and maintained at 37°C body temperature using a heating pad (Stoelting). A dental drill (RWD) was then used to thin the skull at a position 0.95 mm lateral and 0.22 mm caudal to the bregma. A 34G steel needle was inserted into the right lateral ventricle 2.35 mm ventral to the skull surface. A bolus of 2.5 µl of 200 µM P40D680 tracer (Proulx et al., 2013) was infused at the speed of 1 µl/min with a syringe pump (Stoelting). The needle was left in place for 2.5 min and then slowly removed. Ex vivo analysis of brain sections was performed as previously described to ensure proper tracer injection into the lateral ventricle (Ma et al., 2017).

For cisterna magna infusion, a surgical procedure to access this structure was performed as previously described (Ineichen et al., 2017). After a small skin incision was made over the occipital bone/cervical spinal cord, the three covering muscle layers were carefully dissected under a stereomicroscope using fine forceps and scissors. The atlanto-occipital membrane was then prepunctured using a 34G cannula, and the infusion cannula was inserted through this opening into the cisterna magna to a depth of 250 µm. A droplet of histoacryl was added to the interface of cannula and the atlanto-occipital membrane to avoid reflux of CSF during the infusion. Overall, 5 µl of 100 µM P40D680 tracer was infused at the speed of 1 µl/min. After the infusion, the cannula was left in place for 10 min to avoid backflow. After withdrawal of the cannula, a droplet of histoacryl was added to prevent CSF fistula.

In vivo dynamic imaging of tracer flow in the spine
For noninvasive imaging of the spine, fur overlying the thoracic or sacral region of the spine was removed with a razor and depilation cream before tracer infusion. After lateral ventricle tracer infusion, the mice were immediately positioned under a Zeiss StereoLumar.V12 stereomicroscope with AxioVision software (Carl Zeiss) and a Photometrics Evolve 512 camera (Photometrics) in a prone position on a heating pad (37°C). The autofluorescence signal on the GFP channel was used to position the region of the spine at 24× zoom. Dynamic imaging was initiated 5 min after completion of the i.c.v. infusion by acquisition of a sequence of images (one image every 15 s for 55 min) with a Cy5 filter set to monitor the near-infrared signals of the tracers. Exposure time and camera gain settings were 200 ms and 200, respectively.

To assess the tracer transport to the different regions of the spine, a circular region of interest (ROI) with a radius of 500 µm was placed over the spine on the acquired videos. A table of fluorescence intensity in counts versus time was generated using the Measure Profile function and was exported into Microsoft Excel. Baseline intensity in counts was calculated as the average signal of the lowest 10 consecutive imaging frames. This baseline intensity was then subtracted from the fluorescence intensity values to plot fluorescent signal enhancement versus time in minutes. We then examined where the signal starts to climb above this normalized zero value, which indicated the arrival of the tracer at the ROI. To verify that the increase was not due to normal fluctuations in the background signal, we ensured that the signal increased over four consecutive frames. The time point at which the signal increase started was recorded as the transit time of the tracer.

Comparison of CSF dynamics during awake or anesthesia conditions
At 20 min before lateral ventricle infusion, 0.1 mg/kg buprenorphine was injected subcutaneously. Mice were then anesthetized by intraperitoneal injection of 80 mg/kg ketamine and 0.2 mg/kg medetomidine (ket/med group) or by inhalation of 2% isoflurane (awake and isoflurane groups) and fixed in a stereotaxic frame for lateral ventricle tracer infusion (as described above). In the awake group, the mice were allowed to recover (within 5 to 10 min after infusion) and were active for 15, 30, 60, or 90 min (n = 5 each time point). For the ket/med and isoflurane

groups, the mice remained anesthetized for 15, 30, 60, or 90 min on a heating pad (37°C). At the designated times, mice were overdosed by intraperitoneal injection of 400 mg/kg ketamine and 1 mg/kg medetomidine for postmortem imaging.

Analysis of postmortem near-infrared tracer distribution

Images of P40D680 tracer within the CNS-draining LNs and within the spinal column were acquired with a Zeiss AxioZoom V16 microscope and a QImaging OptiMOS sCMOS camera (QImaging) combined with light-emitting diode illumination system pE-4000 (CoolLED) and ZEN 2 software (Carl Zeiss). Images of LNs were acquired in situ at 25× and 200-ms exposure time. Since there were no apparent differences in signal in the LNs on the injected and contralateral sides, the average value of the nodes on each side was used for statistical analysis. The thoracic and sacral regions of the spine were imaged after removal of the skin at 15× and 200-ms exposure time. The region of the thoracic image starts from the junction point of the muscle spinalis and semispinalis thoracis and muscle longissimus thoracis and extends in a caudal direction with the spine in the middle of the image. The region of the sacral region image starts from the base of the tail and extends in a rostral direction with the spine in the middle. For analysis of signal enhancement in the analyzed tissues, background signals were subtracted based on the average signal of three uninjected mice.

Distribution of EB on spinal cord sections

A bolus of 2.5 μl of 0.6% EB (Sigma) was infused in the lateral ventricle (as described above). After 30 min, the mouse was sacrificed, and the spinal cord was carefully dissected out of the spinal column and placed in 4% paraformaldehyde at 4°C for 48 h. Sections at a thickness of 100 μm of spinal cord tissue from the thoracic and lumbar regions were then cut with a vibratome (Leica VT1000 S). Images were acquired with a Zeiss AxioZoom V16 microscope and ZEN 2 software.

Dynamic contrast–enhanced MRI of the spine

20 min before the surgical procedure, mice were injected subcutaneously with carprofen (5 mg/kg). Mice were anesthetized by inhalation of 2% isoflurane and fixed in a stereotaxic frame. Under this narcosis, the skull was thinned with a dental drill, and a 28G, 2.5-mm-long MRI-compatible microcannula (#328OP/PK/Spc; Plastics One) was inserted stereotactically 0.95 mm lateral and 0.22 mm caudal to the bregma and 2.50 mm ventral to the skull surface. Before the infusion, animals were transferred to a horizontal-bore 9.4-T animal scanner (BioSpec Avance III 94/20; Bruker Biospin) with a BGA12S gradient system and ParaVision 6.0.1 (Bruker Biospin). The infusion was performed with a NanoJet syringe pump (Chemyx) pushing a 10-μl Hamilton syringe attached to a 1.5-m PE line. At its opposite end, the line was filled with a 10-μl solution of Gadospin D and connected to the cannula. For whole-spine imaging, a 2-channel transmit/16-channel receive array volume coil with an inner diameter of 60 mm (Bruker Biospin) was used. To limit the size of the pictures and acquisition time, only eight channels were used. Imaging was performed with a 3D time-of-flight gradient recalled echo sequence with repetition/echo time = 14.0/2.5 ms, flip angle = 25°, matrix size = 600 × 216 × 216, field of view = 80.0 ×

28.8 × 28.8 mm, numerical aperture = 2, and t = 6 min 3 s. After one acquisition, a solution of 6 μl Gadospin D at 25 mM gadolinium (nanoPET Pharma) was infused at a rate of 0.1 μl per min. A series of ≥18 scans then continued until ≥108 min. 3D maximum-intensity projection reconstructions were performed with Horos (version 2.0.1, Horos Project). For signal intensity analysis, in Horos software, ROIs were created manually around the sacral spine, sacral LN, and bladder. ROIs were drawn on two sections for each animal, and the signals from each of the anatomical ROIs were averaged. For background determination, circular ROIs were drawn outside the animal body.

Statistical analyses

Statistical analyses were performed with GraphPad Prism 7. Graphs represent mean ± SD. Student's t test was used to compare two groups, and one-way ANOVA followed by the Tukey multiple comparison test was used to compare three groups at each time point. Other types of tests are indicated in the figure legends. A P value <0.05 was considered statistically significant.

Online supplemental material

Fig. S1 demonstrates the differences in CSF tracer distribution after either i.c.v. or i.c.m. infusion to the thoracic and sacral regions of the spine under ket/med anesthesia. Fig. S2 shows P40D680 tracer within additional lymphatic outflow pathways from the lumbar and sacral regions of the spine. Fig. S3 shows the distribution of MR contrast agent Gadospin D over time, including apparent signal within the CC. Video 1 demonstrates noninvasive near-infrared imaging of the thoracic region of the spine after i.c.v. infusion of P40D680, showing signal enhancement in this region over time. Video 2 shows noninvasive near-infrared imaging of the sacral region of the spine after i.c.v. infusion of P40D680, showing an earlier signal enhancement in this region. Video 3 is a 3D dynamic reconstruction of MRI of the CSF contrast agent spread and outflow in the spine.

References

Antila, S., S. Karaman, H. Nurmi, M. Airavaara, M.H. Voutilainen, T. Mathivet, D. Chilov, Z. Li, T. Koppinen, J.H. Park, et al. 2017. Development and plasticity of meningeal lymphatic vessels. *J. Exp. Med.* 214: 3645–3667. https://doi.org/10.1084/jem.20170391

Asgari, M., D.A. de Zélicourt, and V. Kurtcuoglu. 2017. Barrier dysfunction or drainage reduction: differentiating causes of CSF protein increase. *Fluids Barriers CNS.* 14:14. https://doi.org/10.1186/s12987-017-0063-4

Aspelund, A., S. Antila, S.T. Proulx, T.V. Karlsen, S. Karaman, M. Detmar, H. Wiig, and K. Alitalo. 2015. A dural lymphatic vascular system that drains brain interstitial fluid and macromolecules. *J. Exp. Med.* 212: 991–999. https://doi.org/10.1084/jem.20142290

Bachmann, S.B., S.T. Proulx, Y. He, M. Ries, and M. Detmar. 2019. Differential effects of anaesthesia on the contractility of lymphatic vessels in vivo. *J. Physiol.* 597:2841–2852. https://doi.org/10.1113/JP277254

Bakker, E.N., B.J. Bacskai, M. Arbel-Ornath, R. Aldea, B. Bedussi, A.W. Morris, R.O. Weller, and R.O. Carare. 2016. Lymphatic clearance of the brain: perivascular, paravascular and significance for neurodegenerative diseases. *Cell. Mol. Neurobiol.* 36:181–194. https://doi.org/10.1007/s10571-015-0273-8

Boulton, M., A. Young, J. Hay, D. Armstrong, M. Flessner, M. Schwartz, and M. Johnston. 1996. Drainage of CSF through lymphatic pathways and arachnoid villi in sheep: measurement of 125I-albumin clearance. *Neuropathol. Appl. Neurobiol.* 22:325–333. https://doi.org/10.1111/j.1365-2990.1996.tb01111.x

Bozanovic-Sosic, R., R. Mollanji, and M.G. Johnston. 2001. Spinal and cranial contributions to total cerebrospinal fluid transport. *Am. J. Physiol. Regul. Integr. Comp. Physiol.* 281:R909–R916. https://doi.org/10.1152/ajpregu.2001.281.3.R909

Bradbury, M.W.B., and H.F. Cserr. 1985. Drainage of cerebral interstitial fluid and of cerebrospinal fluid into lymphatics. *In Experimental Biology of the Lymphatic Circulation.* M.G. Johnston, editor. Elsevier, Amsterdam. 355–394.

Bradbury, M.W., and W. Lathem. 1965. A flow of cerebrospinal fluid along the central canal of the spinal cord of the rabbit and communications between this canal and the sacral subarachnoid space. *J. Physiol.* 181: 785–800. https://doi.org/10.1113/jphysiol.1965.sp007797

Brierley, J.B., and E.J. Field. 1948. The connexions of the spinal sub-arachnoid space with the lymphatic system. *J. Anat.* 82:153–166.

Cifuentes, M., P. Fernández-LLebrez, J. Pérez, J.M. Pérez-Fígares, and E.M. Rodríguez. 1992. Distribution of intraventricularly injected horseradish peroxidase in cerebrospinal fluid compartments of the rat spinal cord. *Cell Tissue Res.* 270:485–494. https://doi.org/10.1007/BF00645050

Courtice, F.C., and W.J. Simmonds. 1951. The removal of protein from the subarachnoid space. *Aust. J. Exp. Biol. Med. Sci.* 29:255–263. https://doi.org/10.1038/icb.1951.30

Da Mesquita, S., A. Louveau, A. Vaccari, I. Smirnov, R.C. Cornelison, K.M. Kingsmore, C. Contarino, S. Onengut-Gumuscu, E. Farber, D. Raper, et al. 2018. Functional aspects of meningeal lymphatics in ageing and Alzheimer's disease. *Nature.* 560:185–191. https://doi.org/10.1038/s41586-018-0368-8

Davson, H., and M.B. Segal. 1996. *Physiology of the CSF and Blood-Brain Barriers.* CRC Press, Boca Raton, FL. 822 pp.

Di Chiro, G. 1966. Observations on the circulation of the cerebrospinal fluid. *Acta Radiol. Diagn. (Stockh.).* 5(P2):988–1002. https://doi.org/10.1177/02841851660050P242

Dreha-Kulaczewski, S., A.A. Joseph, K.D. Merboldt, H.C. Ludwig, J. Gärtner, and J. Frahm. 2015. Inspiration is the major regulator of human CSF flow. *J. Neurosci.* 35:2485–2491. https://doi.org/10.1523/JNEUROSCI.3246-14.2015

Du Boulay, G., J. O'Connell, J. Currie, T. Bostick, and P. Verity. 1972. Further investigations on pulsatile movements in the cerebrospinal fluid pathways. *Acta Radiol. Diagn. (Stockh.).* 13(0, P2):496–523. https://doi.org/10.1177/02841851720130P205

Elman, R. 1923. Spinal arachnoid granulations with especial reference to the cerebrospinal fluid. *Bull. Johns Hopkins Hosp.* 34:99–104.

Engelhardt, B., P. Vajkoczy, and R.O. Weller. 2017. The movers and shapers in immune privilege of the CNS. *Nat. Immunol.* 18:123–131. https://doi.org/10.1038/ni.3666

Galkin, W.S. 1930. Zur Methodik der Injektion des Lymphsystems vom Subarachnoidalraum aus. *Zeitschr. Ges. Exp. Med.* 74:482–489. https://doi.org/10.1007/BF02624884

Gardner, W.J., and R.J. Goodall. 1950. The surgical treatment of Arnold-Chiari malformation in adults; an explanation of its mechanism and importance of encephalography in diagnosis. *J. Neurosurg.* 7:199–206. https://doi.org/10.3171/jns.1950.7.3.0199

Grundy, H.F. 1962. Circulation of cerebrospinal fluid in the spinal region of the cat. *J. Physiol.* 163:457–465. https://doi.org/10.1113/jphysiol.1962.sp006989

Hsu, M., A. Rayasam, J.A. Kijak, Y.H. Choi, J.S. Harding, S.A. Marcus, W.J. Karpus, M. Sandor, and Z. Fabry. 2019. Neuroinflammation-induced lymphangiogenesis near the cribriform plate contributes to drainage of CNS-derived antigens and immune cells. *Nat. Commun.* 10:229. https://doi.org/10.1038/s41467-018-08163-0

Ineichen, B.V., L. Schnell, M. Gullo, J. Kaiser, M.P. Schneider, A.C. Mosberger, N. Good, M. Linnebank, and M.E. Schwab. 2017. Direct, long-term intrathecal application of therapeutics to the rodent CNS. *Nat. Protoc.* 12: 104–131. https://doi.org/10.1038/nprot.2016.151

Ishibashi, T. 1959. Studies on the dynamics of the cerebrospinal fluid using radioactive isotopes. II. The circulation of cerebrospinal fluid. *Tohoku J. Exp. Med.* 70:59–66. https://doi.org/10.1620/tjem.70.59

Iwanow, G. 1928. Uber die Abflusswege aus den submeningealen Raumen des Ruckenmarks. *Zeitschr. Ges. Exp. Med.* 58:1–21. https://doi.org/10.1007/BF02658191

Jacob, L., L. Boisserand, J. Pestel, S. Antila, J.M. Thomas, M.S. Aigrot, T. Mathivet, S. Lee, K. Alitalo, N. Renier, et al. 2019. Anatomy of the vertebral column lymphatic network in mice. *arXiv* https://arxiv.org/abs/1901.03864v1 (Preprint posted January 12, 2019).

Kida, S., A. Pantazis, and R.O. Weller. 1993. CSF drains directly from the subarachnoid space into nasal lymphatics in the rat. Anatomy, histology and immunological significance. *Neuropathol. Appl. Neurobiol.* 19:480–488. https://doi.org/10.1111/j.1365-2990.1993.tb00476.x

Kido, D.K., D.G. Gomez, A.M. Pavese Jr., and D.G. Potts. 1976. Human spinal arachnoid villi and granulations. *Neuroradiology.* 11:221–228. https://doi.org/10.1007/BF00328377

Koh, L., A. Zakharov, and M. Johnston. 2005. Integration of the subarachnoid space and lymphatics: is it time to embrace a new concept of cerebrospinal fluid absorption? *Cerebrospinal Fluid Res.* 2:6. https://doi.org/10.1186/1743-8454-2-6

Kwon, S., C.F. Janssen, F.C. Velasquez, and E.M. Sevick-Muraca. 2017. Fluorescence imaging of lymphatic outflow of cerebrospinal fluid in mice. *J. Immunol. Methods.* 449:37–43. https://doi.org/10.1016/j.jim.2017.06.010

Leduc, E.H., A.J. Mitchell, and G.B. Wislocki. 1956. On the ending of Reissner's fiber in the filum terminale of the spinal cord. *J. Comp. Neurol.* 104: 493–517. https://doi.org/10.1002/cne.901040307

Liu, S., M.A. Lam, A. Sial, S.J. Hemley, L.E. Bilston, and M.A. Stoodley. 2018. Fluid outflow in the rat spinal cord: the role of perivascular and paravascular pathways. *Fluids Barriers CNS.* 15:13. https://doi.org/10.1186/s12987-018-0098-1

Louveau, A., I. Smirnov, T.J. Keyes, J.D. Eccles, S.J. Rouhani, J.D. Peske, N.C. Derecki, D. Castle, J.W. Mandell, K.S. Lee, et al. 2015. Structural and functional features of central nervous system lymphatic vessels. *Nature.* 523:337–341. https://doi.org/10.1038/nature14432

Louveau, A., J. Herz, M.N. Alme, A.F. Salvador, M.Q. Dong, K.E. Viar, S.G. Herod, J. Knopp, J.C. Setliff, A.L. Lupi, et al. 2018. CNS lymphatic drainage and neuroinflammation are regulated by meningeal lymphatic vasculature. *Nat. Neurosci.* 21:1380–1391. https://doi.org/10.1038/s41593-018-0227-9

Ma, Q., B.V. Ineichen, M. Detmar, and S.T. Proulx. 2017. Outflow of cerebrospinal fluid is predominantly through lymphatic vessels and is reduced in aged mice. *Nat. Commun.* 8:1434. https://doi.org/10.1038/s41467-017-01484-6

Ma, Q., M. Ries, Y. Decker, A. Müller, C. Riner, A. Bücker, K. Fassbender, M. Detmar, and S.T. Proulx. 2019. Rapid lymphatic efflux limits cerebrospinal fluid flow to the brain. *Acta Neuropathol.* 137:151–165. https://doi.org/10.1007/s00401-018-1916-x

Marmarou, A., K. Shulman, and J. LaMorgese. 1975. Compartmental analysis of compliance and outflow resistance of the cerebrospinal fluid system. *J. Neurosurg.* 43:523–534. https://doi.org/10.3171/jns.1975.43.5.0523

McCabe, J.S., and F.N. Low. 1969. The subarachnoid angle: an area of transition in peripheral nerve. *Anat. Rec.* 164:15–33. https://doi.org/10.1002/ar.1091640102

McComb, J.G. 1983. Recent research into the nature of cerebrospinal fluid formation and absorption. *J. Neurosurg.* 59:369–383. https://doi.org/10.3171/jns.1983.59.3.0369

Milhorat, T.H., R.W. Johnson, and W.D. Johnson. 1991. Evidence of CSF flow in rostral direction through central canal of spinal cord in rats. *In Hydrocephalus.* S. Matsumoto and N. Tamaki, editors. Springer-Verlag, Tokyo. pp. 207–217. https://doi.org/10.1007/978-4-431-68156-4_20

Miura, M., S. Kato, and M. von Lüdinghausen. 1998. Lymphatic drainage of the cerebrospinal fluid from monkey spinal meninges with special

reference to the distribution of the epidural lymphatics. *Arch. Histol. Cytol.* 61:277–286. https://doi.org/10.1679/aohc.61.277

Nakayama, Y. 1976. The openings of the central canal in the filum terminale internum of some mammals. *J. Neurocytol.* 5:531–544. https://doi.org/10.1007/BF01175567

O'Connell, J.E.A. 1943. The vascular factor in intracranial pressure and the maintenance of the cerebrospinal fluid circulation. *Brain.* 66:204–228. https://doi.org/10.1093/brain/66.3.204

Post, R.M., F.H. Allen, and A.K. Ommaya. 1974. Cerebrospinal fluid flow and iodide 131 transport in the spinal subarachnoid space. *Life Sci.* 14:1885–1894. https://doi.org/10.1016/0024-3205(74)90405-6

Proulx, S.T., P. Luciani, A. Christiansen, S. Karaman, K.S. Blum, M. Rinderknecht, J.C. Leroux, and M. Detmar. 2013. Use of a PEG-conjugated bright near-infrared dye for functional imaging of rerouting of tumor lymphatic drainage after sentinel lymph node metastasis. *Biomaterials.* 34:5128–5137. https://doi.org/10.1016/j.biomaterials.2013.03.034

Proulx, S.T., Q. Ma, D. Andina, J.C. Leroux, and M. Detmar. 2017. Quantitative measurement of lymphatic function in mice by noninvasive near-infrared imaging of a peripheral vein. *JCI Insight.* 2:e90861. https://doi.org/10.1172/jci.insight.90861

Saker, E., B.M. Henry, K.A. Tomaszewski, M. Loukas, J. Iwanaga, R.J. Oskouian, and R.S. Tubbs. 2016. The human central canal of the spinal cord: a comprehensive review of its anatomy, embryology, molecular development, variants, and pathology. *Cureus.* 8:e927. https://doi.org/10.7759/cureus.927

Voelz, K., D. Kondziella, D.B. von Rautenfeld, T. Brinker, and W. Lüdemann. 2007. A ferritin tracer study of compensatory spinal CSF outflow pathways in kaolin-induced hydrocephalus. *Acta Neuropathol.* 113:569–575. https://doi.org/10.1007/s00401-007-0203-z

Welch, K., and M. Pollay. 1963. The spinal arachnoid villi of the monkeys Cercopithecus aethiops sabaeus and Macaca irus. *Anat. Rec.* 145:43–48. https://doi.org/10.1002/ar.1091450107

Williams, B., and J. Bentley. 1980. Experimental communicating syringomyelia in dogs after cisternal kaolin injection. Part 1. Morphology. *J. Neurol. Sci.* 48:93–107. https://doi.org/10.1016/0022-510X(80)90153-7

Woollam, D.H.M., and J.W. Millen. 1958. Observations on the production and circulation of the cerebrospinal fluid. *In CIBA Foundation Symposium on the Cerebrospinal Fluid.* G.E.W. Wolstenholme and C.M. O'Connor, editors. Little, Brown and Company, Boston. 124-142.

Zenker, W., S. Bankoul, and J.S. Braun. 1994. Morphological indications for considerable diffuse reabsorption of cerebrospinal fluid in spinal meninges particularly in the areas of meningeal funnels. An electronmicroscopical study including tracing experiments in rats. *Anat. Embryol. (Berl.).* 189:243–258. https://doi.org/10.1007/BF00239012